Changes in Ocean Heat Content Caused by Wave–Induced Mixing in a High-Resolution Ocean Model

Article *in* Journal of Physical Oceanography · April 2018

DOI: 10.1175/JPO-D-17-0142.1

5 authors, including:

Kevin Walsh
University of Melbourne
140 PUBLICATIONS **4,649** CITATIONS

SEE PROFILE

Alexander Babanin
University of Melbourne
205 PUBLICATIONS **6,446** CITATIONS

SEE PROFILE

Changes in Ocean Heat Content Caused by Wave-Induced Mixing in a High-Resolution Ocean Model

LACHLAN STONEY

Department of Infrastructure Engineering, University of Melbourne, Melbourne, Victoria, Australia

KEVIN J. E. WALSH

School of Earth Sciences, University of Melbourne, Melbourne, Victoria, Australia

STEVEN THOMAS

Department of Infrastructure Engineering, University of Melbourne, Melbourne, Victoria, Australia

PAUL SPENCE

ARC Centre of Excellence for Climate System Science, and Climate Change Research Centre, University of New South Wales, Kensington, New South Wales, Australia

ALEXANDER V. BABANIN

Department of Infrastructure Engineering, University of Melbourne, Melbourne, Victoria, Australia

(Manuscript received 14 July 2017, in final form 16 March 2018)

ABSTRACT

A parameterization of turbulent mixing from unbroken surface waves is included in a 16-yr simulation within a high-resolution ocean circulation model (MOM5). This ''surface wave mixing'' (SWM) derives from the wave orbital motion and is parameterized as an additional term in a *k*-epsilon model. We show that SWM leads to significant changes in sea surface temperatures but smaller changes in ocean heat content, and show the extent to which these changes can reduce pre-existing model biases with respect to observed data. Specifically, SWM leads to a widespread improvement in sea surface temperature in both hemispheres in summer and winter, while for ocean heat content the improvements are less clear. In addition, we show that introducing SWM can lead to an accumulation of wave-induced ocean heat content between years. While it has been well established that secular positive trends exist in global wave heights, we find that such trends are relatively unimportant in driving the accumulation of wave-induced ocean heat content. Rather, in response to the new source of mixing, the simulated ocean climate evolves toward a new equilibrium with greater total ocean heat content.

1. Introduction

Surface waves can regulate climate by modifying the exchange of heat and momentum between the atmosphere and ocean (see Cavaleri et al. 2012; D'Asaro 2014; D'Asaro et al. 2014). Thermodynamically, the waves can influence climate by altering the characteristics of the air–sea interface, particularly through the generation of bubbles and sea spray during wave breaking (Babanin 2011). Mechanically, the waves can modify vertical mixing processes in the upper ocean when momentum is transferred to the subsurface through wave breaking and Langmuir circulation. Wave breaking, however, only injects turbulence at the scale of wave height (meters) and then relies on vertical diffusion of the turbulence, while Langmuir circulation provides vertical advection of the turbulence at the rate of cm s^{-1}—both the diffusion and advection are much slower than the turbulence vortex turnover and hence the lifetime (e.g., Babanin et al. 2009).

In the meantime, there is turbulence produced by the wave orbital motion, with the wave motion distributed vertically at the scale of the wavelength (about 100 m)

Corresponding author: Kevin Walsh, kevin.walsh@unimelb.edu.au

DOI: 10.1175/JPO-D-17-0142.1

(Babanin 2006, 2017). This can then directly mix through the thermocline without relying on mechanisms of turbulent mixing related to vertical shear or static stability, which are typically included in parameterizations. We denote this additional mixing mechanism as surface wave mixing (SWM). Such wave mixing also represents a thermodynamic effect, in that it contributes to the amount of heat that is mixed down into the ocean (Qiao et al. 2004, 2010; Cavaleri et al. 2012; Toffoli et al. 2012; Ghantous and Babanin 2014a,b; Aijaz et al. 2017; Stoney et al. 2017). Considerable effort has thus gone into representing surface wave processes within numerical models of weather and climate (Song et al. 2007; Babanin et al. 2009; Liu et al. 2011; Chen et al. 2013; Dufresne et al. 2013; Fan and Griffies 2014; Breivik et al. 2015; Li et al. 2016). In addition, significant positive trends in global wave heights have been recently documented (e.g., Young et al. 2011), suggesting the possibility of long-term changes to the energy exchange between the atmosphere and ocean. We note that the observed trends in significant wave heights are positive over most of the globe but particularly so over the Southern Ocean. These trends are also generally larger for extreme events rather than, for example, monthly means (Young et al. 2011).

For the present study, we investigate the possibility of secular changes in ocean heat content (OHC) arising from the mixing induced by unbroken surface waves. The study of OHC variations has become an important diagnostic of circulation changes in the ocean (e.g., Abraham et al. 2013). Changes in OHC also dominate the global energy imbalance due to anthropogenic climate change (Bindoff et al. 2007). The importance of secular trends in wave climate is also explored. Mixing from unbroken surface waves originates from the wave-driven motion itself and is not routinely included in ocean climate models, although it has been examined in some studies (Li et al. 2016). There are three different physical mechanisms for wave-induced turbulence unrelated to wave breaking. The first is due to viscous shear (Phillips 1961; Kinsman 1965), which can generate turbulence at a critical wave-based Reynolds number (Babanin 2006). The other two rely on preexisting turbulence, and since the ocean is always turbulent, they do not need the Phillips mechanism to activate them. Benilov et al. (1993) suggested an instability mechanism for linear two-dimensional potential waves, which can stretch and amplify any preexisting three-dimensional vorticity in the water column (Benilov 2012; Babanin and Chalikov 2012). The empirical and theoretical basis of this wave-induced mixing (see below) is distinct from that of Langmuir turbulence (McWilliams et al. 1997; Teixeira and Belcher 2002). Nevertheless, owing to their different theoretical approaches—with SWM focusing on the wave orbital motions versus Langmuir turbulence approaches based on wave-phase-averaged statistics such as Stokes drift—at present a clear distinction between the two phenomena cannot be made. What is clear, however, is that the scaling law proposed here, being based on orbital velocities (see below), and those proposed for Langmuir turbulence, being based on Stokes drift (e.g., Li et al. 2016), differ in which wave properties are emphasized. It is important to note that both representations of scaling laws agree in that stronger waves lead to stronger mixing. Note also that Langmuir circulation and Langmuir turbulence are not the same phenomena. In theory, it is not completely clear to what extent the SWM and Langmuir processes overlap and interact (Ghantous and Babanin 2014a).

The intensity of the SWM mechanism was found sufficient to describe a number of observed phenomena: sediment suspension in the North Sea (Pleskachevsky et al. 2011), hurricane mixing through the thermocline (Toffoli et al. 2012), and swell decay (Young et al. 2013). On theoretical grounds, SWM is thought to generate significant levels of turbulence at depths of half a wavelength (e.g., 100 m for a wave with a period of 12 s in deep water conditions; Toffoli et al. 2012; Babanin 2017). Evidence for SWM is based on measurements of turbulence beneath unbroken waves in the laboratory (Babanin and Haus 2009; Dai et al. 2010), in the field (Cavaleri and Zecchetto 1987; Toffoli et al. 2012), and in coupled wave–turbulence modeling (Babanin and Chalikov 2012). In addition, several recent studies have shown that the simulation of ocean climate is generally improved when parameterizations of SWM are included (Qiao et al. 2004; Song et al. 2007; Huang et al. 2012; Walsh et al. 2017). However, it must be pointed out that the direct estimation of SWM in the real-world ocean remains controversial owing to the limited number of reliable field observations (D'Asaro 2014; Ghantous and Babanin 2014a).

Thus for the present paper we investigate whether wave trends may be inducing a secular accumulation in global OHC, via the SWM mechanism described above. These are trends for wave height—such trends do exist and have been measured (Young et al. 2011). Trends in wave period (peak frequency) can also affect SWM, but at present stage are unknown (if they exist) and were not investigated. Such an accumulation of OHC would likely be absent in standard climate models in which SWM is not explicitly accounted for. Note that while parameterizations of SWM have been developed and tested previously (Qiao et al. 2004), for the present study we use a relatively new parameterization based on laboratory experiments and observations of swell dissipation. This parameterization was developed by Ghantous and Babanin (2014a) and recently incorporated into an ocean climate model by Walsh et al. (2017).

2. Methods

This study uses a global coupled ocean–sea ice model at mesoscale eddy-permitting resolution that is based on the Geophysical Fluid Dynamics Laboratory (GFDL) Climate Model, version 2.5 (CM2.5) (Delworth et al. 2012). The ocean model is version 5 of the hydrostatic primitive equation Modular Ocean Model (MOM5), and the sea ice model is the GFDL Sea Ice Simulator. Our configuration has 50 vertical levels and a Mercator horizontal grid resolution of approximately 0.25°. Vertical resolution in the upper 100 m is about 10 m, with the closest level to the surface at 5 m. The model was started from initial conditions and equilibrated for 300 years as described by Spence et al. (2014). The atmospheric forcing for this 300-yr run is the CORE-II normal year forcing (Large and Yeager 2009; Griffies 2012), a repeated year of climatological forcing that includes synoptic variability. From this initial condition, the model was forced with the CORE-II interannually varying atmospheric boundary conditions (Large and Yeager 2009; Griffies 2012). We first used this interannual forcing to perform a spinup of two years (1992–93), after which time the upper-ocean temperatures and the global average turbulent kinetic energy became quasi stationary. The experiment runs from 1 January 1994 to 1 January 2010, with a time step of 30 min, using the CORE-II interannual forcing. We stress that all atmospheric fields are prescribed by the CORE-II forcing, and thus there is no feedback to the atmosphere from the ocean. Exchange coefficients of momentum C_d, sensible heat C_e, and latent heat C_h are calculated in MOM5 following the method of Large and Yeager (2004), where they are functions of the neutral stability 10-m wind speed U_{10}. It is worth noting that the surface current is included in the calculation of wind stress and that air temperature, humidity, precipitation, and radiative fluxes are supplied by the atmospheric boundary conditions. Background values of significant wave height and peak wave frequency are supplied hourly from a 30-yr WAVEWATCH III hindcast (Durrant et al. 2014). These data have a horizontal resolution of 0.4° and were then interpolated to the resolution of MOM5.

To represent the ocean vertical mixing we use a one-dimensional mixing model, the General Ocean Turbulence Model (GOTM) (Umlauf and Burchard 2005), incorporated within the MOM modeling system (which is three-dimensional). For the mixing induced by unbroken surface waves, the key element of the present study, we use the parameterization of Ghantous and Babanin (2014a). The parameterization represents the process by which the wave orbital motion itself can amplify preexisting turbulence in the water column. Note that it is not based directly on any of the three theoretical mechanisms described in the introduction, as these are instability theories and so while they predict the growth of turbulence, they do not provide quantitative guidance. The parameterization as formulated here is based on consistent and redundant dimensional (Bowden 1950; Babanin 2011), experimental (Babanin and Haus 2009), numerical (Babanin and Chalikov 2012), and observational (Young et al. 2013) argument and evidence. According to the numerical simulations of Babanin and Chalikov (2012), the level of initial background turbulence is not essential to include in the simulations: if turbulence were not initially seeded, it would even start from digital noise, albeit at a slower rate. Ultimately, its resulting level is determined by the wave energy. This process is included here as an extra term in the k–ε turbulence model (Rodi 1987), one of the many turbulence schemes available in GOTM [see Umlauf et al. (2012, p. 70), for the default parameter values used here]. The k–ε model, widely used in computational fluid dynamics to calculate turbulent kinetic energy (TKE), consists of two equations describing the evolution of TKE, as well as the production and dissipation of that energy. There are two standard source terms, one describing the production from shear processes P and the other production from buoyancy G, respectively, written analytically as follows:

$$P = -u'w'\frac{\partial U}{\partial z} - v'w'\frac{\partial V}{\partial z}, \quad \text{and} \tag{1}$$

$$G = w'b', \tag{2}$$

where u', v', and w' are the zonal, meridional, and vertical turbulent velocities, respectively, U and V are the mean zonal and meridional velocities, and b' is the turbulent buoyancy term. The k–ε model parameterizes the shear production as follows:

$$P = \nu(M^2 + \alpha N^2) + W, \tag{3}$$

where ν is the turbulent viscosity, M is the shear frequency, and αN^2 is a parameterization of the breaking of internal waves, first suggested by Mellor (1989). For this study, we add the new term W to parameterize the wave-induced mixing:

$$W = bk\left(\frac{\omega H_s}{2}e^{kz}\right)^3, \tag{4}$$

where b is an empirical constant set to 0.0014 following Young et al. (2013), k is the wavenumber (calculated from the deep water dispersion relation), ω is the peak

angular frequency, H_s is the significant wave height, and z is the height (zero at the surface and decreasing into the ocean). Here we assume monochromatic waves. The wave-induced turbulence decays exponentially with depth from the surface. Note that in this parameterization the shear frequency remains unaltered when W is introduced, due to the difficulty in clearly separating and parameterizing this effect from observations because of inadequate long-term records of peak wave frequency. Intensity of the turbulence, as described by (4), depends on the waves and does not depend on the initial level of background turbulence, provided it already exists. Otherwise, it can be generated by the Phillips (1961) mechanism as mentioned in the introduction, but this is not necessary, as the ocean is always turbulent.

Various experiments were designed to test the sensitivity of the results to secular trends in the wave climate. In experiment A we calculate the wave-induced anomalies based on two simulations with and without SWM for the years 1994–2009 using the original WAVEWATCH III hindcast. Any trends in the wave hindcast that include the year 1993 are unreliable, because of a well-documented step change in the data assimilation practices at that time (Durrant et al. 2014). This step change is associated with the introduction of surface winds derived from the Special Sensor Microwave Imager (SSM/I) data and the associated reduction in model bias. Thus we have confined our simulations to the January 1994 to January 2010 period, for which the trends in the wave hindcast resemble those calculated from altimeter observations (Young et al. 2011). Experiment B was designed to test the physical significance of secular trends in the wave dataset and differs from experiment A only in that a simple linear trend based on the monthly mean values has been subtracted from the WAVEWATCH III data at each grid point. The trends were calculated from the difference between January 1994 and January 2009. To check that the trends were not sensitive to the specific time period used, we repeated this detrending process with different beginning and end years, as well as with the beginning and end dates moved to July rather than January: the global pattern of linear trends was qualitatively similar in each case. In experiment C we calculate the wave-induced anomalies from two 16-yr simulations with and without SWM, where the atmospheric boundary conditions and wave forcing from the year 1994 are repeated every year to rule out the possibility of secular trends and interannual variability. In experiment C the model state is allowed to evolve continuously during these repeated years of atmospheric forcing (see Table 1 for a summary of experiments).

TABLE 1. Summary of experiments.

Experiment name	Description
Experiment A	Compares simulations with and without SWM
Experiment B	As in experiment A, but with detrended wave inputs
Experiment C	Repeated 1994 boundary conditions, with and without SWM

3. Results

a. Seasonal effects of SWM

A detailed explanation of the seasonal SWM effects around the globe can be found in the study by Walsh et al. (2017), who employed a very similar model setup to that used in the present paper. Here we present an overview of these seasonal effects, which are critical for understanding the secular SWM effects discussed in the next section. Figure 1 shows the specific effect of SWM for each season, averaged over the 1994–2009 simulation period and using the original WAVEWATCH III hindcast (experiment A). In December–January–February (DJF), the Southern Hemisphere summer, the extra mixing from SWM has a cooling effect of 0.5° to 1.0°C close to the surface over much of the Southern Ocean (Fig. 1a). The 5- and 77-m depths were chosen to correspond to the depths of the most significant anomalies in temperature shown (for example) in Fig. 2. This extra mixing corresponds to extra heat mixed down into the thermocline (seen at 77-m depth in Fig. 1b). During June–July–August (JJA), the winter mixed layer in the Southern Ocean becomes very deep, entraining some of the remnant thermocline heat anomalies (i.e., those that are generated in the summer and persist beneath the mixed layer until winter) back toward the surface, leading to slight relative warming near the surface and at 77-m depth (Figs. 1c,d). This relative surface warming is also partly attributable to the extra mixing between the extremely cold surface layer at high latitudes and the slightly warmer mixed layer (Walsh et al. 2017). Very similar patterns are seen in the Northern Hemisphere for the opposite seasons, with the exception that the summer surface cooling due to the inclusion of SWM seen in the high latitudes of the North Pacific and North Atlantic reaches larger peak values (1.0° to 1.5°C cooling) compared to the Southern Ocean.

A different perspective on the seasonal SWM effects in the high latitudes can be seen in Fig. 2, which shows the temperature anomalies from SWM as a function of depth and time for the first five years of the simulation, averaged over the Southern Ocean (50°–70°S). From this

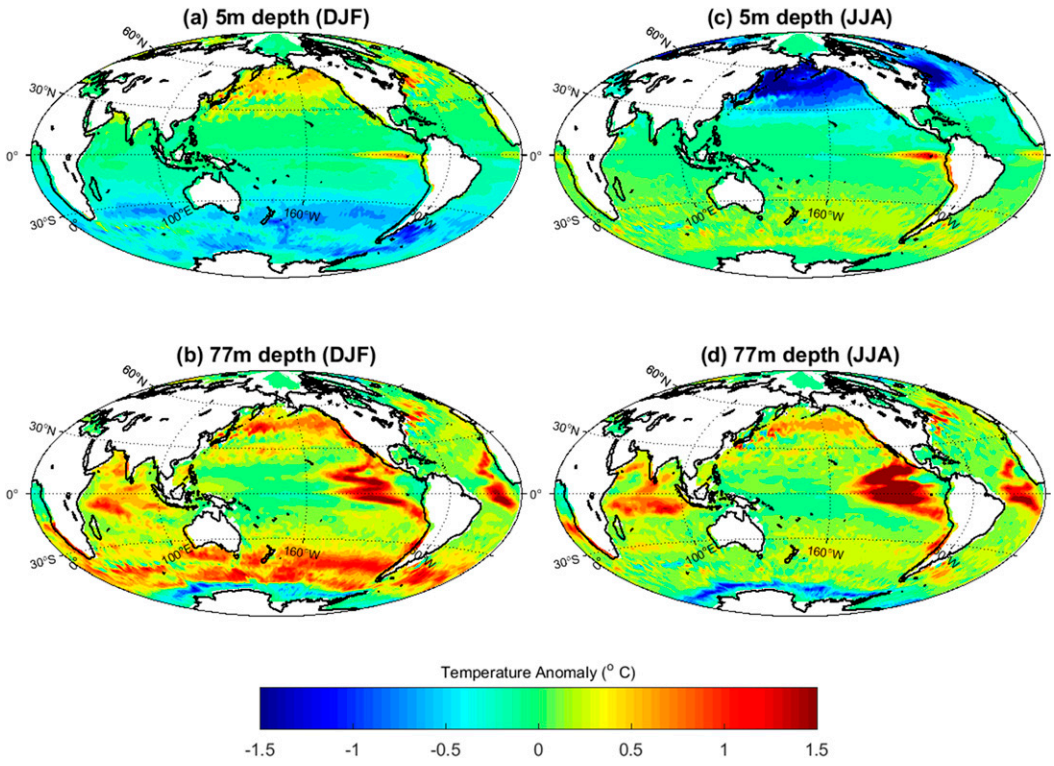

FIG. 1. Average wave-induced temperature anomalies over the simulation period (1994–2009) from experiment A, with labels indicating seasons and depths.

perspective we can see that the summer warming of the thermocline occurs throughout the 50–120-m layer and that the winter warming of the mixed layer seen in Fig. 1 also corresponds to a slight cooling of the 75–200-m layer (this is due to extra mixing of the cold surface layer discussed above). From Fig. 2 it is also clear that many of the seasonal anomalies from SWM persist between the seasons and years: this is particularly obvious with the deeper cool anomalies in the 100–200-m layer and the warm anomalies that migrate between the summer thermocline and the winter mixed layer.

In the equatorial regions, the most obvious effect of SWM is the relative warming of the upwelling zones near the west coasts of South America and Africa (Fig. 1b). At 5-m depth in these regions there is a relative warming effect from SWM of around 0.5° to 1.5°C. These warm anomalies are highly correlated with the positions of the ''cold tongues'' where the absolute surface temperatures are relatively cool. A possible explanation for this effect is changes in horizontal advection. At deeper levels in these regions there is a wave-induced warming effect, where SWM is enhancing the entrainment at the base of the relatively shallow mixed layer (mixed layer depths not shown). This thermocline warming is also present further to the west in both ocean basins, albeit at greater depths than what is shown in Fig. 1 owing to the much deeper mixed layers (not shown). Note that swell waves propagating from higher latitudes are the most likely source of SWM in this region (eastern Pacific), since the local wind speeds are consistently low. This is consistent with the absence of this particular SWM signal in the study of Walsh et al. (2017), who computed the wave heights directly from the local wind speed and thus neglected any effects of swell. Nevertheless, the resolution of the atmospheric forcing and the ocean model used here are coarse compared with that needed for best representation of eastern Pacific upwelling (Small et al. 2014).

Figure 3 shows how the model temperatures at 5-m depth compare with observational data from the *World Ocean Atlas 2009* (*WOA09*) data (Locarnini et al. 2010; Antonov et al. 2010). The model biases (means for DJF and JJA, no waves) are in the range of −3° to 3°C and are mostly positive (Figs. 3a,c). To show how these biases change when SWM is included, we have taken the difference in the absolute values of the errors calculated with and without SWM (Figs. 3b,d). In this figure, negative values indicate reduced bias. In the midlatitudes, the effect of SWM on the model skill is largely positive, with widespread reductions in error of around 0.5°C.

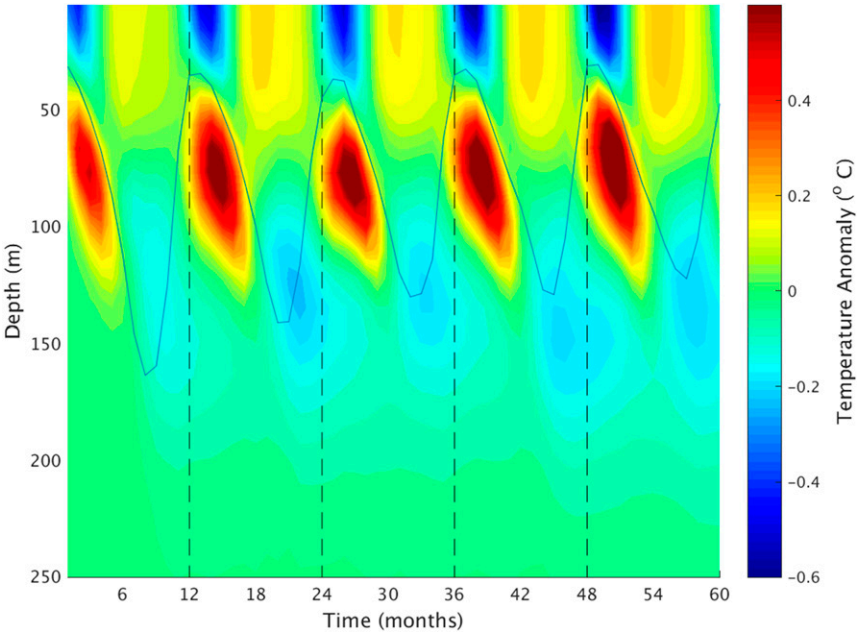

FIG. 2. SWM-induced temperature anomalies (°C) averaged over the Southern Ocean (50°–70°S) from experiment A, for the first five years of simulation (January 1994 to December 1998); *x* axis shows time in months starting at January 1994. The solid line indicates the depth of the mixed layer averaged over the Southern Ocean region, while the dashed lines indicate year boundaries.

In the tropics, the effect of SWM on the model skill is largely neutral, but notably with increases in model error in the upwelling zones in the eastern Pacific and Atlantic. Figure 1 shows that the surface temperature anomaly induced by SWM in the eastern Pacific is positive while the anomaly in the Atlantic upwelling zone is negative. The effect of SWM on the model skill in the 0–300-m layer as a whole is discussed in the next section.

b. *Regional changes in ocean heat content*

Here we investigate the geographical distribution of wave-induced OHC, using the vertically integrated temperature over the 0–300-m layer (approximately the depth below which the SWM effect is negligible; see Fig. 2). Figure 4c shows the existing model biases compared to the *WOA09* data, where the model data are averaged over the simulation period (1994–2009). The *WOA09* data are interpolated to match the MOM5 grid and are displayed for reference in Fig. 4a. Whether the bias is positive or negative is highly variable in space, although it appears that overall there is a slight positive bias. The largest changes in OHC due to SWM (Fig. 4b) appear in the equatorial regions (except in the Indian Ocean) and in the midlatitudes, where the signal is positive. The only region with consistently negative wave-induced OHC is around the Antarctic coast: this reduced OHC corresponds to the wave-induced cool anomalies in the 100–200-m layer discussed in the previous section. The size of the wave-induced signal in OHC (Fig. 4b) is relatively small compared to the corresponding model error (Fig. 4c). Nevertheless, Fig. 4d shows that including SWM can reduce this error in some regions (e.g., the equatorial Pacific), while increasing it in other regions (e.g., Indian Ocean). Since SWM typically increases the local OHC by enhancing vertical mixing, improvements in the simulation tend to occur in those regions that have preexisting negative biases. The reduced OHC around Antarctica, however, also appears to be improving the model simulation of OHC by a small amount.

c. *The effect of secular trends and interannual variability in wave climate*

In this section, we examine the time evolution of wave-induced OHC and investigate the extent to which secular trends in the wave forcing dataset can modify this SWM signal. We test this sensitivity to secular trends in wave climate by repeating the simulations with detrended wave forcing (experiments B and C).

Figure 5 shows the distribution of significant wave height trends in the Southern Hemisphere from the original wave hindcast (experiment A) and from the detrended wave hindcast (experiment B), for the 1994–2009 period. The trends in the original wave hindcast,

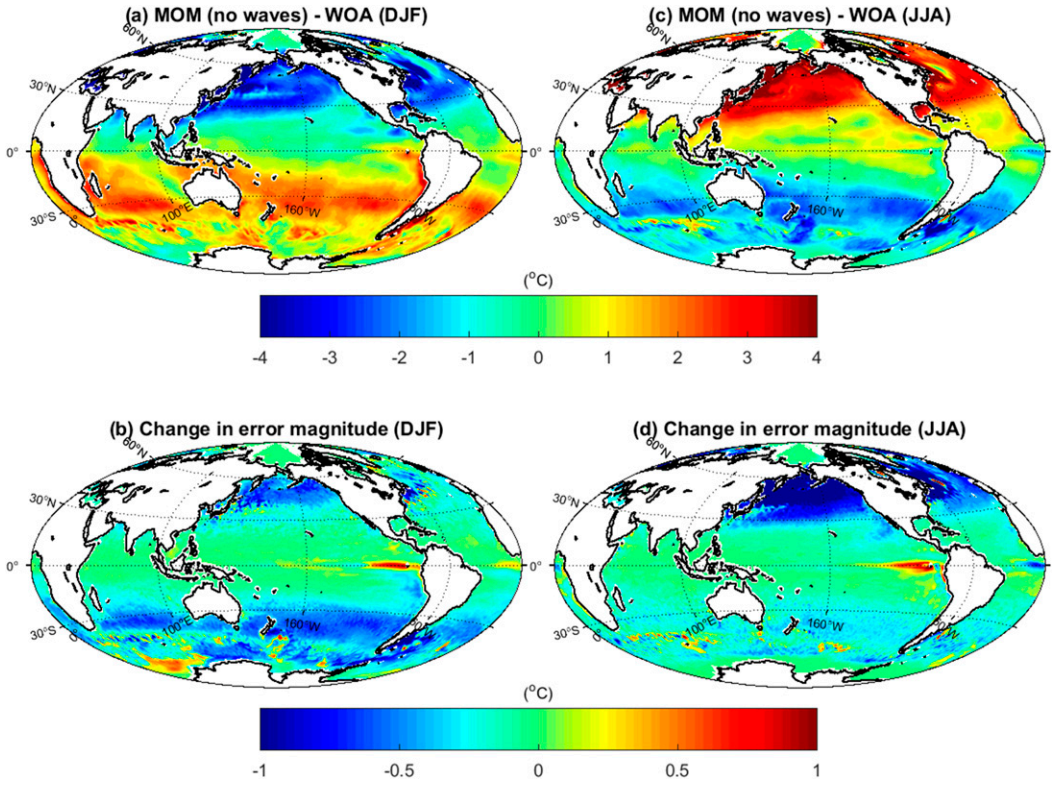

FIG. 3. Comparison to *World Ocean Atlas* data 5-m temperature anomalies, DJF and JJA, for model results averaged over the simulation period (1994–2009); (a),(c) difference between MOM-simulated temperatures with no wave mixing (control) and *WOA09* values; (b),(d) the change in the magnitude of the model biases when wave mixing is included, with negative values indicating less bias.

from both the monthly means and from the monthly 99th-percentile values, are largely positive (0.5% to 1.0% yr^{-1}) over most of the Southern Ocean, particularly in the region just west of the Drake Passage. The trends in the 99th-percentile values show more extreme variation, with generally larger positive trends as well as isolated regions of negative trends that are not obvious in the case of the monthly means. The area of ocean showing statistically significant trends in experiment A is larger for the case of the mean values compared to the extreme values, although in both cases the trends are mostly not statistically significant. For experiment B the mean trend has been subtracted from the wave hindcast at each grid point: this predictably neutralizes most of the trend in the monthly mean wave heights (Fig. 5b), but many of the trends in the 99th-percentile values remain (Fig. 5d). Thus while the wave forcing in experiment B is said to be detrended, there remains some uncertainty about whether the total mixing will still increase over the simulation period, particularly if the extreme wave heights are responsible for an inordinate amount of mixing. Subtracting the trends based on the 99th-percentile values would neutralize the trend in the extreme values but give nonzero trends in the mean values. We then calculate a further trend analysis using the nonparametric seasonal Mann–Kendall test (SKT), to be consistent with Young et al. (2011). This trend analysis method is applied to the wave forcing used in experiment A, which has not been detrended in any way, and the wave forcing used in experiment B, which has already been detrended using the linear regression method described above. This difference in trend estimation is responsible for the isolated regions of apparently nonzero trend in the ''detrended'' wave data (Fig. 5b). Note that the differences in model results are small between this experiment (experiment B) and the no-trend experiment where the year 1994 is repeated for 16 consecutive model years (experiment C). This indicates that the residual trends shown in Fig. 5b have little impact on the final results.

For the wave forcing used in experiment C (the year 1994 repeated for 16 consecutive years), any plots analogous to those in Fig. 5 would of course show zero trend, but it could be argued that the particular choice of year (1994) may not be representative. There is indeed large interannual variability in significant wave heights,

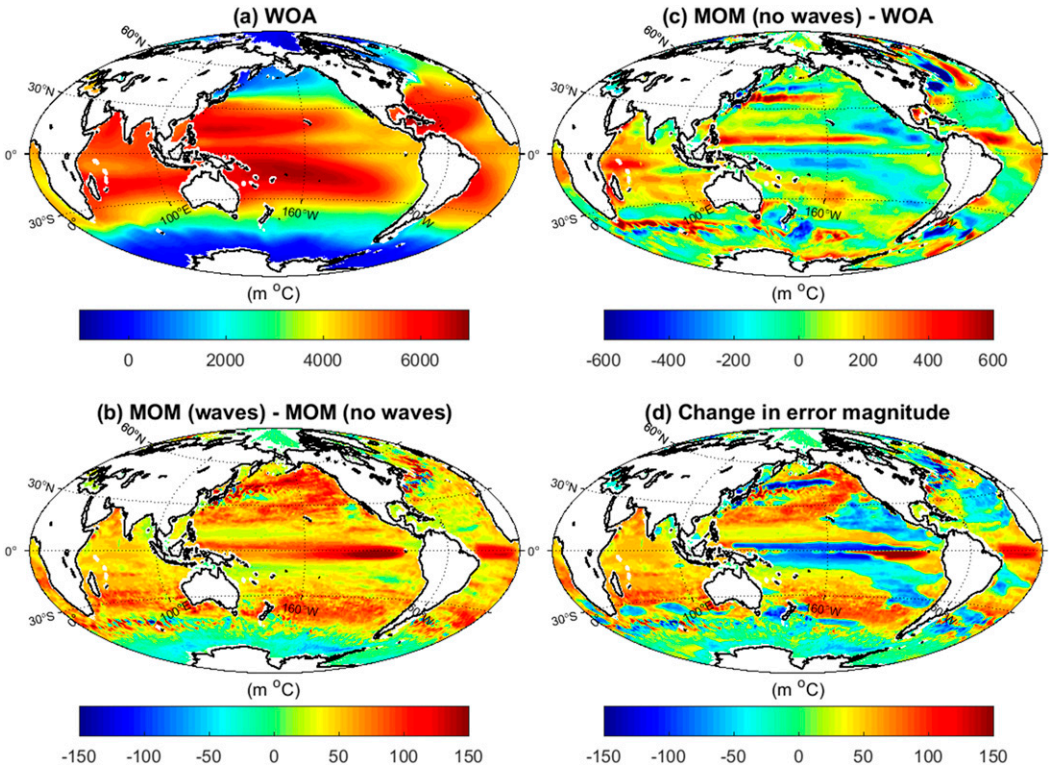

FIG. 4. Comparison to *World Ocean Atlas* data, vertically integrated temperature (0 to 300 m) (in m °C) averaged over the simulation period (1994–2009): (a) *WOA09* values, (b) MOM-simulated biases for the no waves (control) experiment, (c) the differences between the waves and the no waves experiment, and (d) the change in bias due to the introduction of wave mixing, with negative values indicating an improvement.

particularly in the Southern Ocean, yet the mean wave heights for 1994 in both DJF and JJA are about average compared to the other years in the 1994–2009 period (Fig. 6).

Figure 7a shows the total OHC anomaly due to SWM in each experiment, integrated over the entire ocean down to 300-m depth, using

$$\Delta\mathrm{OHC}(t) = c_p \rho_0 \iiint \Delta T(x, y, x, t)\, dx\, dy\, dz,$$

where ΔT is the potential temperature anomaly relative to the control simulation, x is the zonal dimension, y is the meridional dimension, z is height, t is time, and c_p and ρ_0 are the heat capacity and density of seawater, respectively, held constant at $4000\,\mathrm{J\,K^{-1}\,kg^{-1}}$ and $1027\,\mathrm{kg^{-1}\,m^{-3}}$. In spherical coordinates,

$$\Delta\mathrm{OHC}(t) = c_p \rho_0 R^2 \left(\frac{\pi}{180}\right)^2 \iiint \Delta T(\theta, \phi, z, t) \times \cos\phi\, d\phi\, d\theta\, dz,$$

where R is the radius of Earth, ϕ is latitude, and θ is longitude. In all three experiments (A, B, and C), the wave-induced anomaly in total global OHC increases steadily from zero at the beginning of the simulation in 1994, somewhat stabilizing at around 9×10^{22} J by the end of the simulation in 2010. For reference, the mean global OHC (relative to 0°C) in the control simulation from 1994 to 2010 is 5.7×10^{24} J. The accumulation of heat in each experiment progresses as a series of step changes during each Southern Hemisphere summer (DJF). There are only very small differences in the secular rate of accumulation in each experiment, especially between experiments A and B where the only difference is the secular trend (detrended in experiment B). The difference between experiment C and experiment A (or B) is most likely due to the absence of interannual variability in experiment C, rather than any difference in trend. The apparent insensitivity of the wave-induced OHC signal to secular trends suggest that the secular changes in the physical amount of wave-induced mixing are negligible. The specific OHC signal in the Southern Ocean for each experiment is shown in Fig. 7b, showing that in all three experiments the wave-induced OHC reaches a quasi-steady state by the end of the fifth year, varying seasonally between

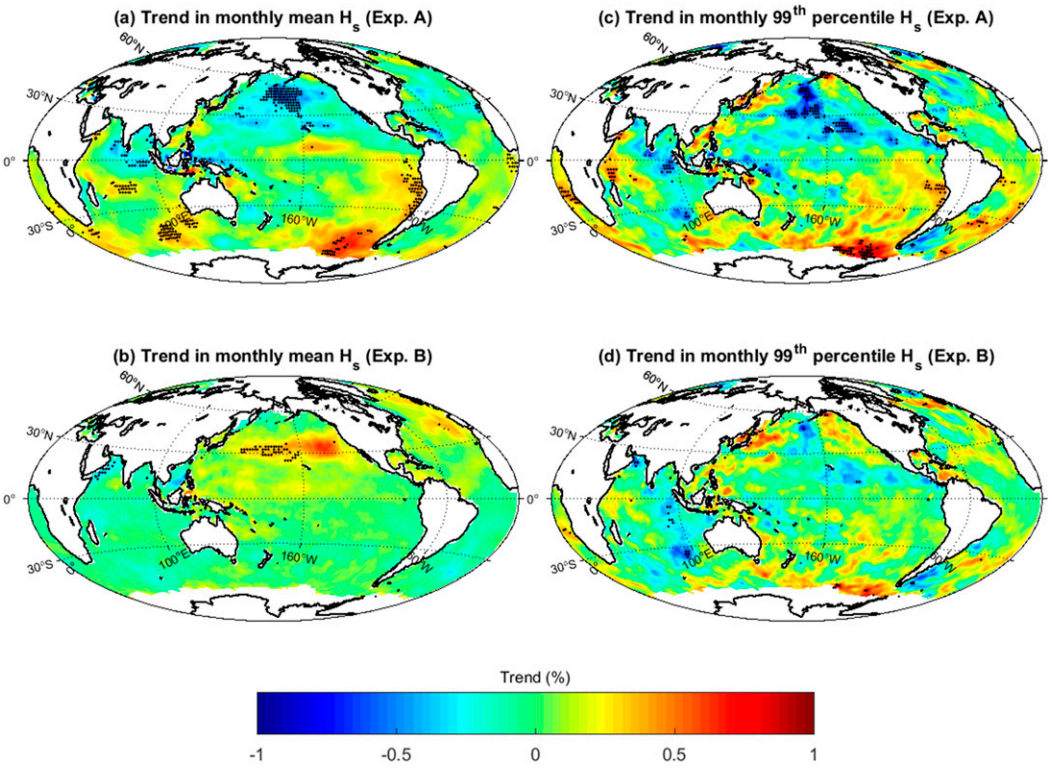

FIG. 5. Trends in significant wave height H_s from the WAVEWATCH III hindcast (top) before (experiment A) and (bottom) after (experiment B) linear detrending. Trend values and statistical significance ($p < 0.05$; black dots) are calculated over the 1994–2009 period according to the SKT. The trends are expressed as percentage changes relative to the mean value at each location over the 1994–2009 period.

2×10^{21} and 12×10^{21} J. For reference, the mean OHC (relative to 0°C) in the Southern Ocean in the control simulation from 1994 to 2010 is 4.2×10^{23} J.

4. Discussion and conclusions

We tested a parameterization of SWM in a high-resolution ocean model (MOM5) and documented the secular physical effects in the ocean. By enhancing the vertical mixing in the upper ocean, SWM can lead to a relative cooling or warming effect that varies with latitude and season. For example, swell propagating across the equator can mix and warm the thermocline. Waves in the Southern Ocean can cool the surface in summer and lead to a slightly warmer surface in winter (relative to a simulation without SWM; see Fig. 2). This extra mixing also generally increases the local OHC in the equatorial and subtropical regions, while near the Antarctic coast the OHC is slightly reduced. Although the wave-induced component of OHC increases steadily over the simulation period (see Fig. 7), we find that this is not a function of any secular change in wave climate, but rather a response of the simulated ocean climate to a new source of mixing. Note also that the different trends in the Southern and Northern Hemisphere wave heights shown in Fig. 5a will lead to a reduced global signal in OHC. Near-identical signals in wave-induced OHC are found regardless of whether or not the wave forcing is detrended over the 16-yr simulation period.

The temperature and heat anomalies caused by SWM can lead to reduced model errors in some regions and increased errors in other regions, when compared with data from the *World Ocean Atlas* (Figs. 3 and 4). For example, the summer SST biases throughout the midlatitudes are generally decreased by around 0.5°C. In the tropics, the effect of SWM on SSTs is largely neutral. SWM generally increases the local OHC, so only those regions with preexisting negative biases in OHC experience corresponding error reductions. Some earlier studies of SWM effects have noted the importance of atmosphere–ocean coupling, which is absent in the present study. For example, Song et al. (2007) showed that including SWM could help reduced a persistent cold bias in the surface equatorial Pacific by facilitating a better representation of the Bjerknes feedback (e.g., Cane 2005) between the ocean and atmosphere.

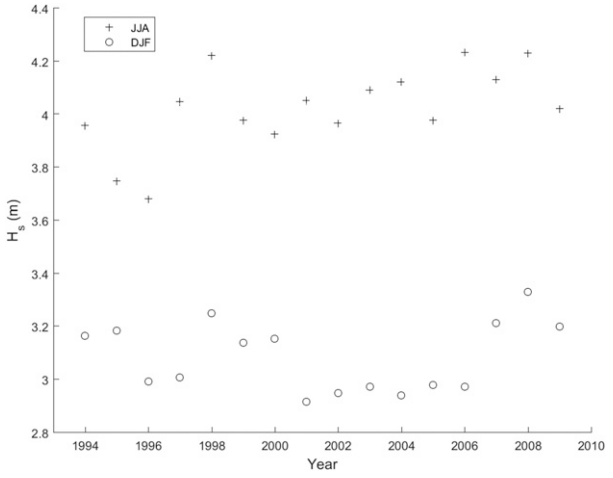

FIG. 6. Mean significant wave heights H_s over the Southern Ocean (40°–70°S) for DJF (circles) and JJA (crosses) from the original WAVEWATCH III hindcast. Year values indicate central month of average (e.g., DJF 1994 corresponds to the average of December 1993, January 1994, and February 1994).

As noted above, a limitation of the experimental design shown here is these are not coupled ocean–atmosphere experiments. Here the atmospheric forcing is specified and there is no feedback from the ocean to the atmosphere. Additionally, the fixed atmosphere will tend to dampen changes in the ocean temperature, likely reducing changes in ocean heat content due to SWM. Thus the experiments here may indicate a lower limit to the ocean response. It would be useful to examine the effect of SWM in a coupled model simulation. A further issue is that the introduction of waves may alter the shear frequency M in (2), although this effect was not incorporated in this study.

It must be pointed out that the tuning of MOM5 (without waves) may in fact implicitly incorporate some SWM effects, if indeed SWM does occur in the real World Ocean. For example, the value of the steady-state Richardson number (Ri = 0.25) sets the vertical mixing profiles in the k-ε model and has been tuned to match observations at ocean weather station (OWS) Papa (Burchard and Bolding 2001). Thus introducing SWM without adjusting any other parameters may be in some sense ''double counting'' the effect of SWM if indeed SWM was an important factor in setting the observed temperature profiles. If this were true, it may go some way in explaining the increased error in OHC caused by introducing SWM, for example, the excessive thermocline warming seen throughout the subtropics in Fig. 4.

In summary, the incorporation of a parameterization of unbroken wave mixing improves the MOM5 simulation of surface temperature, but its effect on the models' simulation

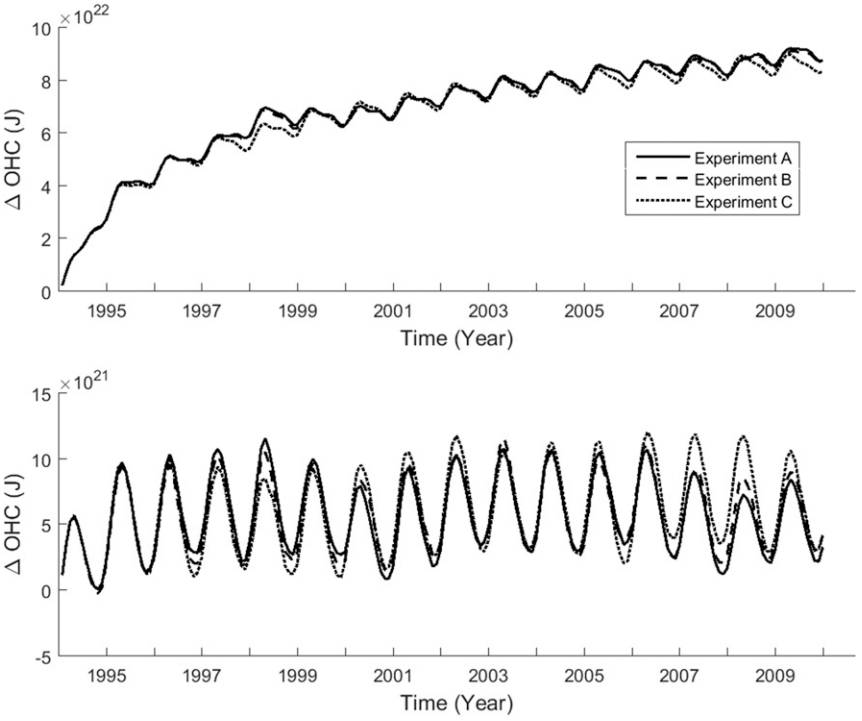

FIG. 7. Wave-induced anomalies in ocean heat content (0 to 300 m) for the (top) globe and (bottom) Southern Ocean (40°–70°S).

of ocean heat content is not as dramatic. Owing to the importance of ocean heat content as a diagnostic of ocean circulation changes, more work is required to investigate the reasons for this discrepancy. Numerous studies have shown an increase in global ocean heat content over the past few decades (Abraham et al. 2013). Changes in ocean heat content constitute about 90% of the total global energy imbalance due to anthropogenic climate change (Bindoff et al. 2007), and thus projections of future changes in this quantity need to be as accurate as possible for the projection of future global temperature changes and sea level rise.

Acknowledgments. The authors thank Nick Hannah and the Consortium of Ocean Sea Ice Modelling in Australia (cosima.org.au) for providing data from their coupled atmosphere–ocean–ice model. This research was undertaken with the assistance of resources from the National Computational Infrastructure (NCI), which is supported by the Australian Government. The authors would particularly like to thank Aiden Heerdegen and Marshall Ward of NCI for their assistance. This work was partially funded by the Australian Research Council Discovery Projects Grant DP 130100227. AVB also acknowledges ARC Discovery Grant DP 170101328 and DISI Australia-China Centre through Grant ACSRF48199. Paul Spence is supported by an Australian Research Council DECRA Fellowship DE150100223. The authors gratefully acknowledge the assistance of Stefan Zieger and Ian Young. All data produced during this work, including the files necessary to reproduce the result, can be obtained on request (kevin.walsh@unimelb.edu.au).

REFERENCES

Abraham, J. P., and Coauthors, 2013: A review of global ocean temperature observations: Implications for ocean heat content estimates and climate change. *Rev. Geophys.*, **51**, 450–483, https://doi.org/10.1002/rog.20022.

Aijaz, S., M. Ghantous, A. V. Babanin, I. Ginis, B. Thomas, and G. Wake, 2017: Nonbreaking wave-induced mixing in upper ocean during tropical cyclones using coupled hurricane-ocean-wave modeling. *J. Geophys. Res. Oceans*, **122**, 3939–3963, https://doi.org/10.1002/2016JC012219.

Antonov, J. I., and Coauthors, 2010: *Salinity*. Vol. 2, *World Ocean Atlas 2009*, NOAA Atlas NESDIS 69, 184 pp.

Babanin, A. V., 2006: On a wave-induced turbulence and a wave-mixed upper ocean layer. *Geophys. Res. Lett.*, **33**, L20605, https://doi.org/10.1029/2006GL027308.

——, 2011: *Breaking and Dissipation of Ocean Surface Waves.* Cambridge University Press, 480 pp.

——, 2017: Similarity theory for turbulence, induced by orbital motion of surface water waves. *Procedia IUTAM*, **20**, 99–102, https://doi.org/10.1016/j.piutam.2017.03.014.

——, and B. K. Haus, 2009: On the existence of water turbulence induced by nonbreaking surface waves. *J. Phys. Oceanogr.*, **39**, 2675–2679, https://doi.org/10.1175/2009JPO4202.1.

——, and D. Chalikov, 2012: Numerical investigation of turbulence generation in nonbreaking potential waves. *J. Geophys. Res.*, **117**, C06010, https://doi.org/10.1029/2012JC007929.

——, A. Ganopolski, and W. R. C. Phillips, 2009: Wave-induced upper-ocean mixing in a climate modelling of intermediate complexity. *Ocean Modell.*, **29**, 189–197, https://doi.org/10.1016/j.ocemod.2009.04.003.

Benilov, A. Y., 2012: On the turbulence generated by the potential surface waves. *J. Geophys. Res.*, **117**, C00J30, https://doi.org/10.1029/2012JC007948.

——, T. G. McKee, and A. S. Safray, 1993: On the vortex instability of the linear surface wave. *Numerical Methods in Laminar and Turbulent Flow*, C. Taylor, Ed., Pineridge, 1323–1334.

Bindoff, N. L., and Coauthors, 2007: Observations: Oceanic climate change and sea level. *Climate Change 2007: The Physical Science Basis*, S. Solomon et al., Eds., Cambridge University Press, 385–428.

Bowden, K. F., 1950: The effect of eddy viscosity on ocean waves. *London Edinburgh Dublin Philos. Mag. J. Sci.*, **41**, 907–917, https://doi.org/10.1080/14786445008561023.

Breivik, Ø., K. Mogensen, J. R. Bidlot, M. A. Balmaseda, and P. A. Janssen, 2015: Surface wave effects in the NEMO ocean model: Forced and coupled experiments. *J. Geophys. Res. Oceans*, **120**, 2973–2992, https://doi.org/10.1002/2014JC010565.

Burchard, H., and K. Bolding, 2001: Comparative analysis of four second-moment turbulence closure models for the oceanic mixed layer. *J. Phys. Oceanogr.*, **31**, 1943–1968, https://doi.org/10.1175/1520-0485(2001)031<1943:CAOFSM>2.0.CO;2.

Cane, M. A., 2005: The evolution of El Niño, past and future. *Earth Planet. Sci. Lett.*, **230**, 227–240, https://doi.org/10.1016/j.epsl.2004.12.003.

Cavaleri, L., and S. Zecchetto, 1987: Reynolds stresses under wind waves. *J. Geophys. Res.*, **92**, 3894–3904, https://doi.org/10.1029/JC092iC04p03894.

——, B. Fox-Kemper, and M. Hemer, 2012: Wind waves in the coupled climate system. *Bull. Amer. Meteor. Soc.*, **93**, 1651–1661, https://doi.org/10.1175/BAMS-D-11-00170.1.

Chen, S. S., W. Zhao, M. A. Donelan, and H. L. Tolman, 2013: Directional wind-wave coupling in fully coupled atmosphere-wave-ocean models: Results from CBLAST-Hurricane. *J. Atmos. Sci.*, **70**, 3198–3215, https://doi.org/10.1175/JAS-D-12-0157.1.

Dai, D., F. Qiao, W. Sulisz, L. Han, and A. Babanin, 2010: An experiment on the nonbreaking surface-wave-induced vertical mixing. *J. Phys. Oceanogr.*, **40**, 2180–2188, https://doi.org/10.1175/2010JPO4378.1.

D'Asaro, E. A., 2014: Turbulence in the upper-ocean mixed layer. *Annu. Rev. Mar. Sci.*, **6**, 101–115, https://doi.org/10.1146/annurev-marine-010213-135138.

——, J. Thomson, A. Y. Shcherbina, R. R. Harcourt, M. F. Cronin, M. A. Hemer, and B. Fox-Kemper, 2014: Quantifying upper ocean turbulence driven by surface waves. *Geophys. Res. Lett.*, **41**, 102–107, https://doi.org/10.1002/2013GL058193.

Delworth, T. L., and Coauthors, 2012: Simulated climate and climate change in the GFDL CM2.5 high-resolution coupled climate model. *J. Climate*, **25**, 2755–2781, https://doi.org/10.1175/JCLI-D-11-00316.1.

Dufresne, J., and Coauthors, 2013: Climate change projections using the IPSL-CM5 Earth System Model: From CMIP3 to CMIP5. *Climate Dyn.*, **40**, 2123–2165, https://doi.org/10.1007/s00382-012-1636-1.

Durrant, T., D. Greenslade, M. Hemer, and C. Trenham, 2014: A global wave hindcast focussed on the central and South Pacific.

Centre for Australian Weather and Climate Research Tech. Rep. 070, 54 pp., http://www.cawcr.gov.au/technical-reports/CTR_070.pdf.

Fan, Y., and S. M. Griffies, 2014: Impacts of parameterized Langmuir turbulence and nonbreaking wave mixing in global climate simulations. *J. Climate*, **27**, 4752–4775, https://doi.org/10.1175/JCLI-D-13-00583.1.

Ghantous, M., and A. V. Babanin, 2014a: Ocean mixing by wave orbital motion. *Acta Phys. Slovaca*, **64**, 1–57.

——, and ——, 2014b: One-dimensional modelling of upper ocean mixing by turbulence due to wave orbital motion. *Nonlinear Processes Geophys.*, **21**, 325–338, https://doi.org/10.5194/npg-21-325-2014.

Griffies, S. M., 2012: Elements of the Modular Ocean Model (MOM). GFDL Ocean Group Tech. Rep. 7, 620 pp., http://www.mom-ocean.science/web/docs/project/MOM5_manual.pdf.

Huang, C. J., F. Qiao, Q. Shu, and Z. Song, 2012: Evaluating austral summer mixed-layer response to surface wave-induced mixing in the Southern Ocean. *J. Geophys. Res.*, **117**, C00J18, https://doi.org/10.1029/2012JC007892.

Kinsman, B., 1965: *Wind Waves: Their Generation and Propagation on the Ocean Surface*. Prentice Hall, 676 pp.

Large, W. G., and S. G. Yeager, 2004: Diurnal to decadal global forcing for ocean and sea-ice models: The data sets and flux climatologies. NCAR Tech. Note NCAR/TN-460+STR, 105 pp., https://doi.org/10.5065/D6KK98Q6.

——, and ——, 2009: The global climatology of an interannually varying air–sea flux data set. *Climate Dyn.*, **33**, 341–364, https://doi.org/10.1007/s00382-008-0441-3.

Li, Q., A. Webb, B. Fox-Kemper, A. Craig, G. Danabasoglu, W. G. Large, and M. Vertenstein, 2016: Langmuir mixing effects on global climate: WAVEWATCH III in CESM. *Ocean Modell.*, **103**, 145–160, https://doi.org/10.1016/j.ocemod.2015.07.020.

Liu, B., H. Liu, L. Xie, C. Guan, and D. Zhao, 2011: A coupled atmosphere–wave–ocean modeling system: Simulation of the intensity of an idealized tropical cyclone. *Mon. Wea. Rev.*, **139**, 132–152, https://doi.org/10.1175/2010MWR3396.1.

Locarnini, R. A., A. V. Mishonov, J. I. Antonov, T. P. Boyer, H. E. Garcia, O. K. Baranova, M. M. Zweng, and D. R. Johnson, 2010: *Temperature*. Vol. 1, *World Ocean Atlas 2009*, NOAA Atlas NESDIS 68, 184 pp.

McWilliams, J. C., P. P. Sullivan, and C.-H. Moeng, 1997: Langmuir turbulence in the ocean. *J. Fluid Mech.*, **334**, 1–30, https://doi.org/10.1017/S0022112096004375.

Mellor, G. L., 1989: Retrospect on oceanic boundary layer modeling and second moment closure. *Parameterization of Small-Scale Processes: Proc. 'Aha Huliko'a Hawaiian Winter Workshop*, Honolulu, HI, University of Hawai'i at Mānoa, 251–271.

Phillips, O. M., 1961: A note on the turbulence generated by gravity waves. *J. Geophys. Res.*, **66**, 2889–2893, https://doi.org/10.1029/JZ066i009p02889.

Pleskachevsky, A., M. Dobrynin, A. V. Babanin, H. Gunther, and E. Stanev, 2011: Turbulent mixing due to surface waves indicated by remote sensing of suspended particulate matter and its implementation into coupled modeling of waves, turbulence, and circulation. *J. Phys. Oceanogr.*, **41**, 708–724, https://doi.org/10.1175/2010JPO4328.1.

Qiao, F., Y. Yuan, Y. Yang, Q. Zheng, C. Xia, and J. Ma, 2004: Wave-induced mixing in the upper ocean: Distribution and application to a global ocean circulation model. *Geophys. Res. Lett.*, **31**, L11303, https://doi.org/10.1029/2004GL019824.

——, ——, T. Ezer, C. Xia, Y. Yang, X. Lu, and Z. Song, 2010: A three-dimensional surface wave-ocean circulation coupled model and its initial testing. *Ocean Dyn.*, **60**, 1339–1355, https://doi.org/10.1007/s10236-010-0326-y.

Rodi, W., 1987: Examples of calculation methods for flow and mixing in stratified fluids. *J. Geophys. Res.*, **92**, 5305–5328, https://doi.org/10.1029/JC092iC05p05305.

Small, R. J., and Coauthors, 2014: A new synoptic scale resolving global climate simulation using the Community Earth System Model. *J. Adv. Model. Earth Syst.*, **6**, 1065–1094, https://doi.org/10.1002/2014MS000363.

Song, Z., F. Qiao, Y. Yang, and Y. Yuan, 2007: An improvement of the too cold tongue in the tropical Pacific with the development of an ocean-wave-atmosphere coupled numerical model. *Prog. Nat. Sci.*, **17**, 576–583, https://doi.org/10.1080/10020070708541038a.

Spence, P., S. Griffies, M. England, A. Hogg, O. Saenko, and N. Jourdain, 2014: Rapid subsurface warming and circulation changes of Antarctic coastal waters by poleward shifting winds. *Geophys. Res. Lett.*, **41**, 4601–4610, https://doi.org/10.1002/2014GL060613.

Stoney, L., K. Walsh, A. V. Babanin, M. Ghantous, P. Govekar, and I. R. Young, 2017: Simulated ocean response to tropical cyclones: The effect of a novel parameterization of mixing from unbroken surface waves. *J. Adv. Model. Earth Syst.*, **9**, 759–780, https://doi.org/10.1002/2016MS000878.

Teixeira, M. A. C., and S. E. Belcher, 2002: On the distortion of turbulence by a progressive surface wave. *J. Fluid Mech.*, **458**, 229–267, https://doi.org/10.1017/S0022112002007838.

Toffoli, A., J. McConochie, M. Ghantous, L. Loffredo, and A. V. Babanin, 2012: The effect of wave-induced turbulence on the ocean mixed layer during tropical cyclones: Field observations on the Australian north-west shelf. *J. Geophys. Res.*, **117**, C00J24, https://doi.org/10.1029/2011JC007780.

Umlauf, L., and H. Burchard, 2005: Second-order turbulence closure models for geophysical boundary layers: A review of recent work. *Cont. Shelf Res.*, **25**, 795–827, https://doi.org/10.1016/j.csr.2004.08.004.

——, K. Bolding, and H. Burchard, 2012: GOTM scientific documentation, version 4.0. General Ocean Turbulence Model Group Rep., 346 pp.

Walsh, K., P. Govekar, A. Babanin, M. Ghantous, and P. Spence, 2017: The effect on simulated ocean climate of a parameterization of unbroken wave-induced mixing incorporated into the k-epsilon mixing scheme. *J. Adv. Model. Earth Syst.*, **9**, 735–758, https://doi.org/10.1002/2016MS000707.

Young, I. R., S. Zieger, and A. V. Babanin, 2011: Global trends in wind speed and wave height. *Science*, **332**, 451–455, https://doi.org/10.1126/science.1197219.

——, A. V. Babanin, and S. Zieger, 2013: The decay rate of ocean swell observed by altimeter. *J. Phys. Oceanogr.*, **43**, 2322–2333, https://doi.org/10.1175/JPO-D-13-083.1.